Determining light distribution in human head using 3D Monte Carlo simulations

Böcklin, C ; Baumann, D ; Keller, E ; Fröhlich, J

Abstract: Near Infrared (NIR) extinction measurements can be used to determine the cerebral hemodynamics of adult patients. To be able to interpret and verify measurement data, it is necessary to know the three-dimensional light intensity distribution in the human head. This light intensity map can advantageously be created by numerical simulations. Such simulations of light intensity in the head are complex, since the light is crossing several tissue types with very distinct optical properties. The Monte-Carlo method proved to represent a reliable tool for simulation of light intensity in turbid media. The desired result of a Monte-Carlo simulation is the spatially resolved average light intensity, which has to be derived from the statistical output of the Monte-Carlo simulation. We propose a novel analysis method which directly tracks the intensity based on a line-drawing algorithm to attain a 3D intensity map of the whole computational domain. The proposed method largely operates independently of the underlying Monte-Carlo algorithm itself. The algorithm is verified through comparison with analytical approximations of the Radiative Transport Equation. As a challenging example, the simulation of the light intensity distribution inside the human head based on segmented MRI data is presented.

DOI: https://doi.org/10.1117/12.909155

Determining light distribution in human head using 3D Monte Carlo simulations

Christoph Böcklin[a], Dirk Baumann[a], Emanuela Keller[b], Jürg Fröhlich[a]

[a]Laboratory for Electromagnetic Fields and Microwave Electronics, ETH Zurich, Switzerland
[b]Neurocritical Care Unit, Department of Neurosurgery, University Hospital Zurich, Switzerland

ABSTRACT

Near Infrared (NIR) extinction measurements can be used to determine the cerebral hemodynamics of adult patients. To be able to interpret and verify measurement data, it is necessary to know the three-dimensional light intensity distribution in the human head. This light intensity map can advantageously be created by numerical simulations. Such simulations of light intensity in the head are complex, since the light is crossing several tissue types with very distinct optical properties. The Monte-Carlo method proved to represent a reliable tool for simulation of light intensity in turbid media. The desired result of a Monte-Carlo simulation is the spatially resolved average light intensity, which has to be derived from the statistical output of the Monte-Carlo simulation. We propose a novel analysis method which directly tracks the intensity based on a line-drawing algorithm to attain a 3D intensity map of the whole computational domain. The proposed method largely operates independently of the underlying Monte-Carlo algorithm itself. The algorithm is verified through comparison with analytical approximations of the Radiative Transport Equation. As a challenging example, the simulation of the light intensity distribution inside the human head based on segmented MRI data is presented.

Keywords: Monte Carlo, radiative transport

1. INTRODUCTION

Optical diagnosis has always been a pivotal part of detection and recognition of diseases in medicine. With modern laser technology, light can be exploited for treatment and monitoring of various kinds of diseases. Lasers are not only used in diagnosis, surgical aid or even cancer treatment, light is also employed in medical imaging, such as optical tomography or functional brain imaging. A technology attracting a lot of attention recently, is near infrared (NIR) extinction measurements. Since the early 1970s, NIR extinction measurements are applied for pulse oximetry at the finger and towards the end of the 1970s they were proposed to monitor cerebral hemodynamics. Nowadays, this is done either in a minimal invasive approach[1] which has the major advantage that the light is transmitted and received directly in the white matter without being influenced by other areas of the head. Or, following an non-invasive approach, laser light is emitted from a patch placed on the scalp and thus has to pass through skin, skull, cerebrospinal fluid (CSF) layer, meninges and grey matter before it reaches white matter. Unfortunately, these intermediate tissue layers distort the light signal significantly. Therefore, it is important to investigate and understand the distribution of the average light intensity in the whole area of interest. Since the structure of the head is complex and contains areas with very different optical properties, the only feasible approach to investigate light distribution are numerical simulations. The goal is to obtain a three-dimensional average intensity map of the head to be able to interpret measurement data of hemodynamics.

Light propagation in tissue is generally described by the Radiative Transport Equation (RTE). This equation can not be solved in a closed form, but analytical approximations exist for the two cases where either diffusion or absorption prevails. Various studies have used the diffusion equation[2] with different adaptations[3] or hybrid approaches[4,5] to analyze light propagation and reflection in head models. In contrast, the Monte-Carlo (MC) method offers a universal approach to simulate light distribution in highly heterogeneous media with arbitrary optical parameters. However, MC simulations do not inherently yield the average light intensity. The intensity must be derived from the paths of the photons launched in a MC simulation. Most of the Monte-Carlo algorithms presented until now store the photon absorption and derive the average intensity from this relative absorption

Author contact: C. Böcklin, boecklic@ifh.ee.ethz.ch

grid. Although this approach is straightforward, it is unpractical for materials with a low absorption coefficient. We are interested in a general procedure to generate intensity maps in arbitrary materials and for this reason we introduce a new intensity-analysis algorithm, which is tracking the photon paths and which can be independently applied on top of general MC simulations. The principle problem behind tracing of a photon path in a regular grid is well known in computer graphics as "line drawing". We use a three-dimensional adaptation of the Bresenham line-drawing algorithm which serves as a fast and stable approach to track the path of photon packets. The underlying main 3D MC algorithm has been developed from scratch. It incorporates established MC theory[6–13] and can handle arbitrary geometries and material distributions. The proposed intensity-tracking algorithm is verified by comparison with approximative solutions of the RTE for highly absorbing and highly scattering materials.

In order to achieve a satisfactory approximation of the RTE, a huge number of photon packets is required, resulting in a heavy computational burden. This obstacle is overcome with a parallelized code exploiting today's multicore systems. For this work we favor a Message Passing Interface (MPI) parallelization which is advantageous because the serial code can be parallelized with little extra effort. Finally, as a challenging example, the proposed algorithm is employed to create a three-dimensional map of light average intensity in the adult head based on MRI data.

2. LIGHT PROPAGATION IN TURBID MEDIA

The theory for a heuristic description of light propagation in turbid media was initiated already in 1905.[14] The RTE is generally describing the transport of energy through a material containing particles and is applied to various problems in different areas, as e.g. underwater visibility, radiant energy in the atmospheres of stars and galaxies[15] and also light transport in tissue

$$\frac{\mathrm{d}I(\vec{\mathbf{r}},\hat{\mathbf{s}})}{\mathrm{d}s} = -\mu_t I(\vec{\mathbf{r}},\hat{\mathbf{s}}) + \frac{\mu_t}{4\pi}\int_{4\pi} p(\hat{\mathbf{s}},\hat{\mathbf{s}}')I(\vec{\mathbf{r}},\hat{\mathbf{s}}')\mathrm{d}\omega'. \tag{1}$$

The total extinction coefficient $\mu_t = \mu_a + \mu_s$ is the sum of the absorption coefficient μ_a and the scattering coefficient μ_s. $I(\vec{\mathbf{r}},\hat{\mathbf{s}})$ $[\mathrm{W/m^2 \cdot sr}]$ is called specific intensity or radiance and describes the distribution of photon power per unit area at position $\vec{\mathbf{r}}$ in direction $\hat{\mathbf{s}}$.[15] Since absorption of light in tissue occurs irrespective of the incident direction, the fluence rate or average intensity $\phi(\vec{\mathbf{r}})$ is of more interest in the area of biomedical optics and radiotherapy. The average intensity is the integration of the specific intensity over all solid angles ω

$$\phi(\vec{\mathbf{r}}) = \int_{4\pi} I(\vec{\mathbf{r}},\hat{\mathbf{s}})\mathrm{d}\omega. \tag{2}$$

From the RTE we can identify two parts which contribute to the change in radiance. The first part accounts for the decrease in radiance at point $\vec{\mathbf{r}}$ in direction $\hat{\mathbf{s}}$ due to scattering and absorption. The second part describes the increase of the fluence rate $I(\vec{\mathbf{r}},\hat{\mathbf{s}})$ due scattering from $\hat{\mathbf{s}}$' into $\hat{\mathbf{s}}$. Scattering here means the mere directional deflection of radiance since the interaction is assumed to be completely elastic and hence no energy is consumed or deposited.

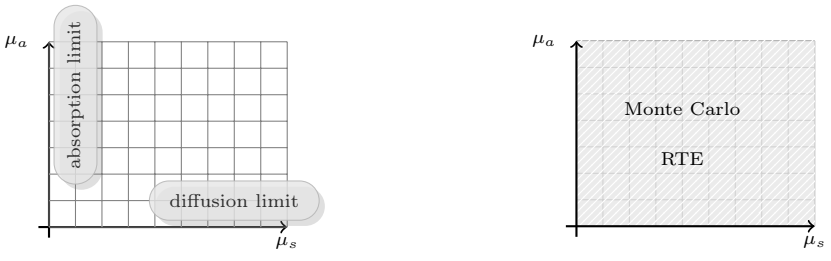

(a) (b)

Figure 1: (a) Validity of the analytical approximations of the RTE in the material parameter space. (b) Validity of the RTE and MC simulations.

The RTE can not be solved in a closed form. For the two extreme cases, where either absorption or scattering prevails, analytical approximations exist (see Figure 1a). For highly absorbing materials ($\mu_a \gg \mu_s$) the Lambert law[16] serves as an approximation of the RTE. In Cartesian coordinates it reads as follows

$$\phi(x,y,z) = P_0 \frac{\exp(-\mu_a \cdot \sqrt{x^2+y^2+z^2})}{4\pi \cdot (x^2+y^2+z^2)} \quad \left[\frac{\mathrm{W}}{\mathrm{m}^2}\right], \tag{3}$$

where P_0 is the power amplitude of the source. Strictly this is only valid if $\mu_s = 0$.

For highly scattering materials ($\mu_s \gg \mu_a$), the diffusion equation[15] can be derived from the RTE. For an isotropic point source its solution is given by

$$\phi(x,y,z) = \frac{P_0 3\mu_{\mathrm{eff}}}{4\pi} \frac{\exp(-\sqrt{3\mu_a\mu_{\mathrm{eff}}} \cdot \sqrt{x^2+y^2+z^2})}{4\pi\sqrt{x^2+y^2+z^2}} \quad \left[\frac{\mathrm{W}}{\mathrm{m}^2}\right], \tag{4}$$

where ϕ is the fluence rate and P_0 is the power amplitude of the source. The effective transport coefficient is $\mu_{\mathrm{eff}} = \mu_s(1-g)+\mu_a$. The anistropy coefficient $g = \langle\cos\theta\rangle$ is given by the expectation value of the scattering angle θ of the phase function $p(\hat{\mathbf{s}}, \hat{\mathbf{s}}')$ which is commonly approximated by the Henyey-Greenstein phase function.[17]

3. AVERAGE-INTENSITY TRACKING ALGORITHM

For a general solution of the RTE, numerical methods have to be applied. A successful approach to solve the RTE numerically is the Monte-Carlo method. Monte-Carlo methods sample a given physical quantity statistically. In the case of the RTE, this quantity is the average intensity $\phi(\vec{\mathbf{r}})$. A MC simulation hence simply creates a spatially resolved relative probability of the intensity. It is tempting to employ the picture of simulating the path of individual photons in a Monte-Carlo simulation. However, it is the nature of MC simulations that single events do not have a physical meaning, but only the resulting probability distribution has. For simplicity we will nevertheless use the term "photon packet", representing one statistical sample of the average intensity. The MC simulation itself does not conceptually rely on a discretized computational space. If the underlying geometry contains arbitrary spatial material distributions, a strong coupling to the geometrical grid is however inevitable.

The simulation analysis is decoupled from the simulation domain bringing along great flexibility for the evaluation of the simulation. The simulation analysis can comprise several different methods at the same time, for example the absorption and average intensity can be tracked in parallel. In contrast to the MC simulation, spatially resolved results for the absorption and average intensity indispensably require a grid, which can be arbitrarily defined. Yet, when working with MRI data, it is an obvious choice to use the same grid dimensions as provided by the MRI data. Figure 2 illustrates the flexibility and decoupling of the analysis domain from computational domain. In Figure 2a, an example of a cubical computational space is shown. The grey square represents the plane, where a photon packet is propagating. Figure 2b shows the photon path in a magnified view of this plane. The tracking of the photon path employing the Bresenham line drawing algorithm is shown in Figure 2c.

3.1 Absorption Tracking

Whenever the weight of a photon packet is reduced (due to absorption), the absorbed weight w_a is added to the cell corresponding to the photon packet's current position $[i,j,k]$ in the absorption grid. By normalizing with the total number of simulated photon packets N_t one obtains a relative absorption probability

$$P_{A[i,j,k]} = \frac{A_{[i,j,k]}}{V_{[i,j,k]} \cdot N_t \cdot W_p}\ , \tag{5}$$

where $V_{[i,j,k]}$ is the volume of the cell $[i,j,k]$, W_p is the initial weight of a photon packet and $A_{[i,j,k]}$ is the sum of all absorption events in the cell $[i,j,k]$.

This is the usual procedure for MC simulations. Although the average intensity ϕ can be computed from the number of absorbed photons $\phi = P_A/\mu_a$,[10] this is unpractical for materials with low absorption coefficients μ_a since during a large portion of the simulation time nothing is contributed to the result. In the example we present in the end this holds in particular for the CSF layer. The value of the absorption and hence the fluence furthermore depends on the analysis-grid spacing. To achieve a similar statistical accuracy a larger amount of photons has to be simulated when the analysis-grid spacing is decreased (i.e. the resolution increased).

3.2 Average-Intensity Tracking

We are interested in a universal method to analyze Monte-Carlo simulations independently of the material parameters and the analysis-grid spacing. In order to obtain the light average intensity we track the total photon path in an intensity grid rather than single absorption events. The intensity grid can hereby have an arbitrary spacing. This procedure is very similar to line drawing in bitmap images. The Bresenham line-drawing algorithm[18] is an efficient way to determine the pixels (or cells in our case) which are covered by a line (photon path). The Bresenham algorithm is borrowed and adapted to the needs in a Monte-Carlo simulation. The 3D adaption[19] of a Bresenham line-drawing algorithm[20] is employed in our implementation. As illustrated in Figure 2c, the cells being crossed by a photon path are determined based on this algorithm. The photon weight

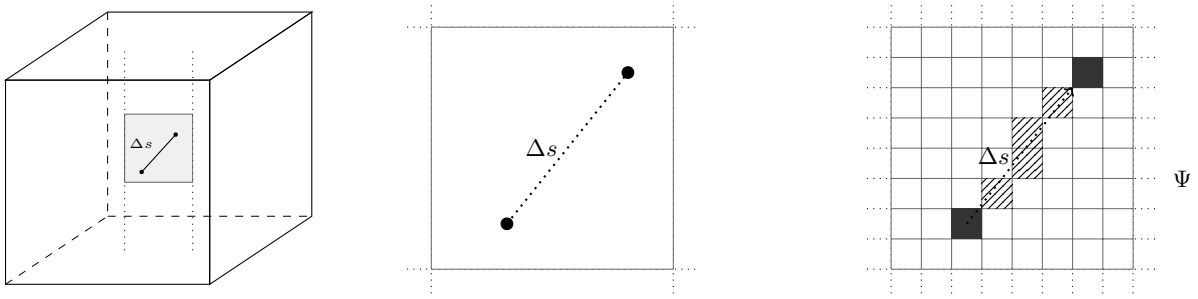

(a) (b) (c)

Figure 2: (a) MC cubic computational domain with highlighted example of a photon step in the grey plane. (b) Photon step (magnified view) in the computational domain. (c) Photon step tracked by Bresenham line-drawing algorithm in the intensity grid.

w_p is then added in the fluence rate grid Ψ to each crossed cell which has been identified by the Bresenham algorithm. The relative fluence is determined by

$$P_{\phi_{[i,j,k]}} = \frac{\Psi_{[i,j,k]}}{V_{[i,j,k]} \cdot N_t \cdot W_p}, \tag{6}$$

where $V_{[i,j,k]}$ is the volume of the cell $[i,j,k]$, N_t is the total number of simulated photon packets, W_p is the initial weight of a photon packet and $\Psi_{[i,j,k]}$ is the sum of all fluence events in the cell $[i,j,k]$.

3.3 Validation

The average intensity analysis of the MC simulation is compared to the analytical approximations of the RTE presented in section 2. The rational is that if the Monte-Carlo simulation is able to reproduce the approximations of the RTE in those two regimes ($\mu_a \gg \mu_s$ and $\mu_s \gg \mu_a$), it is able to generally solve the RTE for all possible combinations of μ_s and μ_a.

Figure 3b shows the setup for the comparison analysis. A Monte-Carlo simulation of a cubical computational domain with a side length $A = 10\,\mathrm{cm}$ and filled with a homogeneous material is performed. An isotropic point source is located in the center. The average intensity is tracked in a regular grid and is evaluated on the diagonal of the computational domain. The analysis grid has the resolution D and the spacing $\Delta a = A/D$. Due to the detachment of the simulation and the average-intensity analysis grid, different grid resolutions D can be analyzed within the same MC simulation.

The values obtained from the average-intensity analysis grid are a probability of the intensity averaged over the cell size of the grid. These values are compared to the analytical solution averaged over the same cells size, which is computed as follows

$$\overline{\Phi}_{[i,j,k]} = \frac{1}{V_{[i,j,k]}} \cdot \int_{x_i}^{x_i+\Delta x} \int_{y_j}^{y_j+\Delta y} \int_{z_k}^{z_k+\Delta z} \phi(x,y,z)\mathrm{d}x\mathrm{d}y\mathrm{d}z \quad \left[\frac{\mathrm{W}}{\mathrm{m}^2}\right]. \tag{7}$$

(a) (b)

Figure 3: (a) Computational domain employed for comparison of MC simulations with analytical approximations. An isotropic point source is located in the center of the domain. (b) Cells where the average intensity computed with the analytical approximations are compared to the MC simulation results.

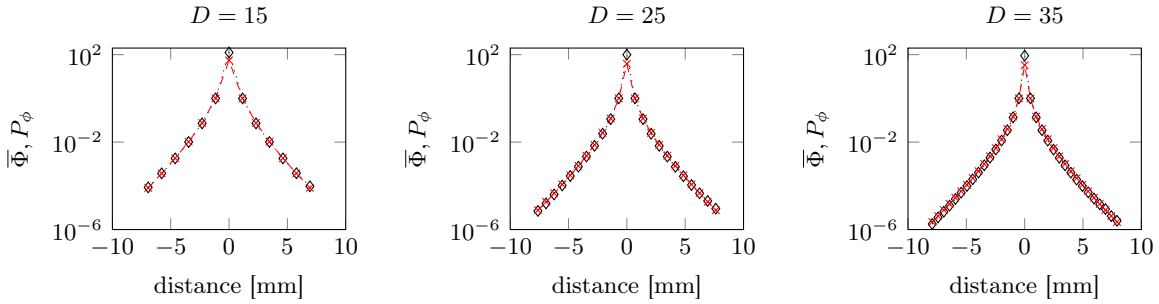

Figure 4: Comparing MC results (◇) with Lambert law (×) for various grid dimensions

Figure 4 shows the comparison between the MC simulations and the cell-averaged analytical solution for different grid dimensions D. The curves are normalized to the value in the cell which is adjacent to the source cell. The material values for this comparison are $\mu_a = 1.0/\,\mathrm{mm}$, $\mu_s = 0.0001/\,\mathrm{mm}$ and $g = 0.0$. The agreement between the analytical solution and the MC simulation is very good for all of the different grid spacings.

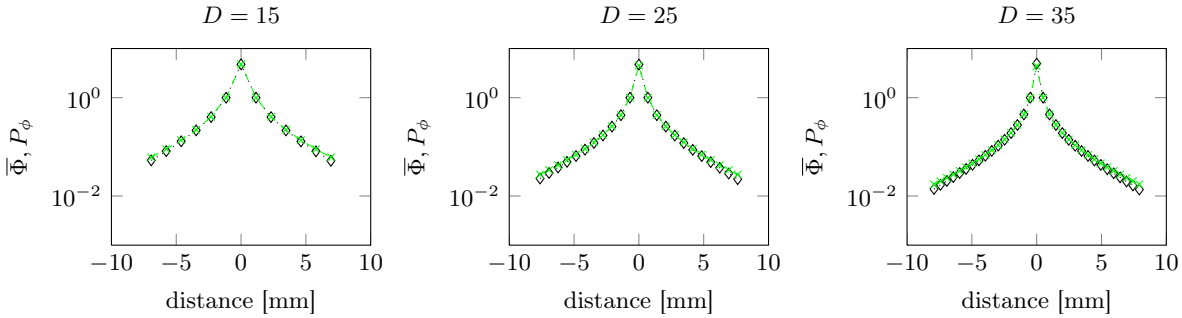

Figure 5: Comparing MC results (◇) with diffusion equation (×) for various grid dimensions

Figure 5 shows the comparison between the MC simulation and the cell-averaged diffusion equation for grid dimensions D. The curves are normalized to the value in the cell which is adjacent to the source cell. The material values for this comparison are $\mu_a = 0.001/\,\mathrm{mm}$, $\mu_s = 10.0/\,\mathrm{mm}$ and $g = 0.0$. Also for diffuse media, the agreement between the analytical solution and the MC simulation is very good, irrespective of the chosen grid spacing.

3.4 Implementation

The core of the developed MC code is a fully object-oriented shared library written in C++ with an interface to the python script language. An important piece of a Monte-Carlo simulator is the random number generator (RNG). Here, the RNGs available in the GNU Scientific Library[21] are employed. A Mersenne-Twister-based[22]

	μ_a [mm^{-1}]	μ_s [mm^{-1}]	g	Reference
Skin	0.015	18	0.9	Simpson[33]
Skull	0.025	28	0.92	Firbank[34]
CSF	0.001	0.01	0.99	assumption
White/Grey Matter	0.02	50.0	0.9	van der Zee[35]
Ventricle	2.0	70.0	0.99	Roggan[36]

Table 1: Optical properties of tissue types present in the human head.

generator is sufficiently fast and has a very long period (2^{19937}). Each process of the simulator has its own RNG engine seeded with the individual process number. The Visualization Toolkit[23] is used for visualization of the results and description of the input geometries. Results are also saved as binary Matlab® files, allowing for a fast and easy analysis of the data.

One major burden of MC simulations are the generally high computational costs since achieving small statistical errors requires a huge amount of simulation events. In the context of the RTE, this number additionally depends on simulation parameters like the size of the computational domain and the optical parameters of the tissues. Improvements to the speed can be achieved on the algorithmic side with for example the photon packet technique or programming optimizations like replacing the computation of trigonometric functions with approximations.[24] Yet, in order to be able to simulate large volumes like the human head it is inevitable to parallelize the code to achieve reasonable simulation times. Recent implementations make use of graphics card processors (GPU) which provide large numbers of parallel threads.[11,25,26] In the framework presented here, a message passing interface (MPI)[27] parallelization scheme has been implemented. Such, processes can be spread over different machines in a cluster and adaptations to the code are not necessary if the environment changes. Monte-Carlo algorithms are very appreciative for parallelization, since they consist of series of independent processes which do not depend on results from previous processes. Still, care has to be taken at the step of data reduction at the end of a simulation. The parallelized code speeds up virtually linear with the number of processes (cores) available.

4. INTENSITY DISTRIBUTION IN HUMAN HEAD

For an accurate monitoring of the hemodynamics of the brain based on NIR extinction monitoring, it is paramount to know the exact light average intensity distribution inside the human head. For this reason, different studies have been performed on simplified layered head models.[2,28–30] These studies have investigated for example the reflected light of the structure or the partial optical path lengths in the different tissue types. Employing more advanced computational models, recent publications show results based on structural data obtained by MRI and CT.[10,11,31]

In the example presented in the following, the light average intensity distribution inside a detailed model of the human head is presented. Our MC code and analysis algorithm presented in this paper are used in order to determine a 3D average intensity map. The input data for the simulation is constructed using an MRI dataset of the head. It is segmented using image processing algorithms available in the open source program *Seg3D2*.[32] The segmented dataset distinguishes five different regions, namely skin, skull, cerebrospinal fluid, grey/white matter and the ventricle region. For this simulation, the segmented volume data is cut into 8 parts and only one segment serves as input data. The optical properties that are employed for the different tissue types in the simulation are listed in Table 1.

A point source is placed on the surface of the skin tissue and emits light in direction of the center of the head. Figure 6 shows the average intensity plotted on the surface of the skull (left) and on the surface of the grey/white matter (right). The relative average intensity is plotted in logarithmic scale (arbitrary units). The results show that the average intensity rapidly drops inside the head and only a small fraction of the light reaches the grey and white matter. The structure is simulated on a Linux computer using 20 Xeon CPUs with 2.67 GHz clock each. The simulation for 10^{10} photon packets on this computer takes approximately $20h$. Figure 7 shows how the statistical error is decreasing with increasing number of photons. After each doubling of the number of photons, the relative intensity is compared to the previous step. The absolute error in cell $[i, j, k]$ is

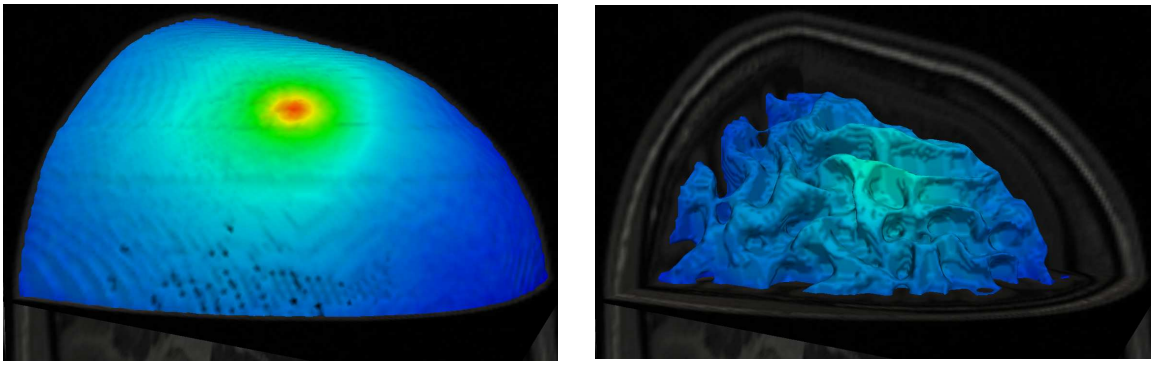

Figure 6: Relative Intensity plotted on the surface of the skull (left) and grey/white matter (right) (logarithmic color space)

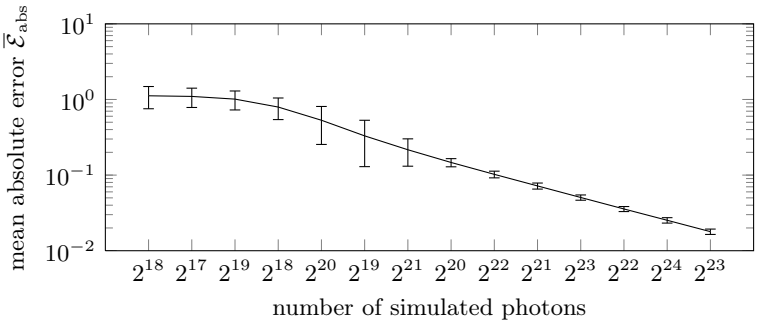

Figure 7: The mean statistical error computed after every doubling of the number of simulated photons.

computed by $\mathcal{E}_{\text{abs}}^{[i,j,k]} = |\Psi_{[i,j,k]}^{N}/\Psi_{[i,j,k]}^{N-1} - 2|$, where 2^N is the number of photons. The mean error $\overline{\mathcal{E}}_{\text{abs}}$ is defined as $\mathcal{E}_{\text{abs}}^{[i,j,k]}$ averaged over all cells of the intensity grid. After 10^{10} photons, the statistical error has decreased to approximately $2 \cdot 10^{-2}$.

5. CONCLUSION

In the context of NIR extinction measurements the determination of the light average intensity in the whole computational domain is the desired result of MC simulations. Whereas most MC simulations are based on absorption tracking algorithms, we proposed a new average intensity tracking algorithm. The presented approach tracking the average intensity offers great flexibility, because it operates independently of the underlying MC simulation. The average intensity tracking algorithm has been successfully verified by comparison with analytical approximations of the RTE. Our MC code is parallelized and hence allows the simulation of complex and large structures in reasonable time while achieving a small statistical error. A segmented MRI dataset of a human head served as an example to demonstrate the capability of the versatile framework to simulate light distribution in complex structures.

REFERENCES

[1] Keller, E., Froehlich, J., Muroi, C., Sikorski, C., and Muser, M., "Neuromonitoring in intensive care: A new brain tissue probe for combined monitoring of intracranial pressure (icp) cerebral blood flow (cbf) and oxygenation," *Acta Neurochir Suppl.* **110**(2), 217–220 (2011).

[2] Koyama, T., Iwasaki, A., Ogoshi, Y., and Okada, E., "Practical and adequate approach to modeling light propagation in an adult head with low-scattering regions by use of diffusion theory," *Applied optics* **44**(11), 2094–2103 (2005).

[3] Arridge, S. R., Dehghani, H., Schweiger, M., and Okada, E., "The finite element model for the propagation of light in scattering media: A direct method for domains with nonscattering regions," *Medical Physics* **27**(1), 252–264 (2000).

[4] Hayashi, T., Kashio, Y., and Okada, E., "Hybrid monte carlo-diffusion method for light propagation in tissue with a low-scattering region," *Appl. Opt.* **42**, 2888–2896 (Jun 2003).

[5] Ma, G., Delorme, J.-F., Gallant, P., and Boas, D. A., "Comparison of simplified monte carlo simulation and diffusion approximation for the fluorescence signal from phantoms with typical mouse tissue optical properties," *Appl. Opt.* **46**, 1686–1692 (Apr 2007).

[6] Prahl, S. A., Keijzer, M., Jacques, S. L., and Welch, A. J., "A monte carlo model of light propagation in tissue," in [*SPIE Proceedings of Dosimetry of Laser Radiation in Medicine and Biology*], **IS 5**, 102–111 (1989).

[7] Wang, L. and Jacques, S., "Monte carlo modeling of light transport in multi-layered tissues in standard c," *The University of Texas, MD Anderson Cancer Center, Houston* (1992).

[8] Wang, L., Jacques, S. L., and Zheng, L., "MCML - Monte Carlo modeling of light transport in multi-layered tissues," *Computer Methods and Programs in Biomedicine* **47**, 131–146 (1995).

[9] Jacques, S. and Wang, L., "Monte carlo modeling of light transport in tissues," *Optical-thermal response of laser-irradiated tissue* , 73–100 (1995).

[10] Boas, D., Culver, J., Stott, J., and Dunn, A., "Three dimensional monte carlo code for photon migration through complex heterogeneous media including the adult human head," *Opt. Express* **10**(3), 159–170 (2002).

[11] Fang, Q. and Boas, D. A., "Monte carlo simulation of photon migration in 3d turbid media accelerated by graphics processing units," *Optics Express* **17**, 20178–20190 (October 2009).

[12] Pfefer, T., Barton, J., Chan, E., Ducros, M., Sorg, B., Milner, T., Nelson, J., and Welch, A., "A three-dimensional modular adaptable grid numerical model for light propagation during laser irradiation of skin tissue," *IEEE Journal of Selected Topics in Quantum Electronics* **2**(4) (1996).

[13] Binzoni, T., Leung, T., Giust, R., Rüfenacht, D., and Gandjbakhche, A., "Light transport in tissue by 3d monte carlo: Influence of boundary voxelization," *Computer Methods and Programs in Biomedicine* **89**(1), 14 – 23 (2008).

[14] Schuster, A., "Radiation through a foggy atmosphere," *The astrophysical journal* **21**, 1 (1905).

[15] Ishimaru, A., [*Wave Propagation and Scattering in Random Media*], IEEE Press (1997).

[16] Lambert, J., [*Photometria, sive de Mensura et gradibus luminis, colorum et umbrae*], sumptibus viduae E. Klett (1760).

[17] Henyey, L. G. and Greenstein, J. L., "Diffuse radiation in the galaxy," *Astroph. J.* **93**, 70–83 (1941).

[18] Bresenham, J., "Algorithm for computer control of a digital plotter," *IBM Systems journal* **4**(1), 25–30 (1965).

[19] Pendleton, B., "line3d." ftp://ftp.isc.org/pub/usenet/comp.sources.unix/volume26/line3d (1992).

[20] Heckbert, P. S., "Graphics gems," ch. Digital line drawing, 99–100, Academic Press Professional, Inc., San Diego, CA, USA (1990).

[21] Galassi, M., Gough, B., Jungman, G., Theiler, J., Davies, J., Booth, M., and Rossi, F., *The GNU Scientific Library Reference Manual*, 3 ed. (2007).

[22] Matsumoto, M. and Nishimura, T., "Mersenne twister: a 623-dimensionally equidistributed uniform pseudo-random number generator," *ACM Trans. Model. Comput. Simul.* **8**, 3–30 (January 1998).

[23] Schroeder, W., Martin, K., and Lorensen, B., [*The Visualization Toolkit: An Object-Oriented Approach To 3D Graphics*], Prentice Hall (1997).

[24] Żołek, N. S., Liebert, A., and Maniewski, R., "Optimization of the Monte Carlo code for modeling of photon migration in tissue," *Computer Methods and Programs in Biomedicine* **84**(1), 50 – 57 (2006).

[25] Alerstam, E., Svensson, T., and Andersson-Engels, S., "Parallel computing with graphics processing units for high-speed monte carlo simulation of photon migration," *Journal of Biomedical Optics* **13**(6), 060504 (2008).

[26] Ren, N., Liang, J., Qu, X., Li, J., Lu, B., and Tian, J., "Gpu-based monte carlo simulation for light propagation in complex heterogeneous tissues," *Opt. Express* **18**, 6811–6823 (Mar 2010).

[27] Gabriel, E., Fagg, G. E., Bosilca, G., Angskun, T., Dongarra, J. J., Squyres, J. M., Sahay, V., Kambadur, P., Barrett, B., Lumsdaine, A., Castain, R. H., Daniel, D. J., Graham, R. L., and Woodall, T. S., "Open MPI: Goals, concept, and design of a next generation MPI implementation," in [*Proceedings, 11th European PVM/MPI Users' Group Meeting*], 97–104 (September 2004).

[28] Hoshi, Y., Shimada, M., Sato, C., and Iguchi, Y., "Reevaluation of near-infrared light propagation in the adult human head: implications for functional near-infrared spectroscopy," *Journal of Biomedical Optics* **10**(6), 064032 (2005).

[29] Okada, E. and Delpy, D., "Near-infrared light propagation in an adult head model. i. modeling of low-level scattering in the cerebrospinal fluid layer," *Applied Optics* **42**(16), 2906–2914 (2003).

[30] Okada, E., Firbank, M., Schweiger, M., Arridge, S. R., Cope, M., and Delpy, D. T., "Theoretical and experimental investigation of near-infrared light propagation in a model of the adult head," *Applied Optics* **36**, 21–31 (January 1997).

[31] Fukui, Y., Ajichi, Y., and Okada, E., "Monte carlo prediction of near-infrared light propagation in realistic adult and neonatal head models," *Appl. Opt.* **42**, 2881–2887 (Jun 2003).

[32] "Seg3d: Volumetric image segmentation and visualization," (2007-2011). Scientific Computing and Imaging Institute (SCI) (http://www.seg3d.org).

[33] Simpson, C. R., Kohl, M., Essenpreis, M., and Cope, M., "Near-infrared optical properties of ex vivo human skin and subcutaneous tissues measured using the monte carlo inversion technique," *Physics in Medicine and Biology* **43**(9), 2465 (1998).

[34] Firbank, M., Hiraoka, M., Essenpreis, M., and Delpy, D., "Measurement of the optical properties of the skull in the wavelength range 650-950 nm," *Physics in Medicine and Biology* **38**, 503 (1993).

[35] van der Zee, P., Essenpreis, M., and Delpy, D., "Optical properties of brain tissue," in [*Proceedings of SPIE*], **1888**(1993) (1993).

[36] Roggan, A., Friebel, M., Dörschel, K., Hahn, A., and Müller, G., "Optical properties of circulating human blood in the wavelength range 400-2500 nm," *Journal of Biomedical Optics* **4**, 36–46 (January 1999).